GEOPHYSICS, VOL. 68, NO. 4 (JULY-AUGUST 2003); P. 1232–1240, 5 FIGS.
10.1190/1.1598115

Transient field solution for a layer of finite thickness on a resistive basement

Bension Sh. Singer* and Andrew Green‡

ABSTRACT

A closed-form asymptotic solution is derived for the magnetic field of the currents induced by a transient airborne magnetic source in a conductive layer of finite thickness. The conductive layer rests on top of a resistive half-space. Like the well-known solution found by J. C. Maxwell for a thin conductive sheet surrounded by an insulator, the secondary magnetic field is expressed in terms of an image source receding from the layer. However, the new solution also accounts for the layer thickness h and the conductivity of the half-space.

One of the conclusions from the new solution is that the mirror plane that specifies the position of the image is located below the upper interface of the conductive layer at depth $h/3$. This indicates the correct position at which the equivalent thin sheet should be placed when Maxwell's solution is applied to a layer of finite thickness.

If the basement that underlies the layer is highly resistive, Maxwell's solution becomes accurate when induced currents are almost uniformly spread across the layer. It remains accurate as long as currents induced in the basement can be neglected. Eventually, the secondary magnetic field of these currents will prevail over the field of currents in the layer. Maxwell's solution loses its accuracy long before this occurs. Depending on parameters of the model, the validity time range of Maxwell's solution may be narrow or even nonexistent.

The generalized image solution is applicable in the time range $h/v_s < t < (\sigma_s/\sigma_b)(h/v_s)$, where v_s is the image recession speed, and σ_s and σ_b are the layer and basement conductivities, respectively. This range is significantly wider than that of Maxwell's solution. At early times, the secondary magnetic field is controlled by the position of the nearest interface of the conductive layer. Accounting for this observation, a simple modification of the new solution may be used to extend the applicability range towards even earlier times. The generalized solution is faster by several orders of magnitude than a numeric solution based on successive wavenumber-to-space and frequency-to-time domain fast Hankel transforms.

INTRODUCTION

The well-known transient solution found by Maxwell over a century ago (e.g., Maxwell, 1954) for a planar homogeneous thin conductive sheet surrounded by an insulator and energized by a magnetic dipole is widely used for interpretation of airborne electromagnetic data. In that solution, the source dipole moment is zero up to moment $t = 0$; then, it changes to a nonzero value and remains constant afterwards. The step change in the primary magnetic field induces an electric current in the conductor. In its turn, the induced current develops a secondary magnetic field. Above the conductive layer, the secondary magnetic field is equivalent to the field of another magnetic dipole located on the other side of the thin sheet. The magnetic moment of this dipole has the same absolute value as the source dipole; its orientation and initial position coincide with a mirror image of the source. But, as time increases, it recedes from the conductive layer at constant speed:

$$v_s = \frac{2}{\mu_0 S}, \tag{1}$$

where S is the layer conductance, and $\mu_0 = 4\pi \times 10^{-7}$ H/m is the free-space magnetic permeability.

Maxwell's solution can be used for any external magnetic source (i.e., for an arbitrary closed circulation of current flowing above the conductive layer). From the step response, a solution can be found for an arbitrary time behavior of the source. The Maxwell's solution is widely used as a kernel function for interpretation of transient electromagnetic (TEM)

Presented at the 69th Annual International Meeting, Society of Exploration Geophysicists. Manuscript received by the Editor March 30, 1999; revised manuscript received February 27, 2003.
*Formerly Cooperative Research Center for Australian Mineral Exploration, Sydney, Australia; presently CSIRO Petroleum, ARRC, P.O. Box 1130, Bentley, Western Australia 6102, Australia. E-mail: benison.singer@csiro.au.
‡Formerly Cooperative Research Center for Australian Mineral Exploration, Sydney, Australia; presently OTBC Pty. Ltd, 8 Lawley Cres., Pymble, New South Wales 2073, Australia. E-mail: greenaa@ozemail.com.au.

soundings and airborne transient data over layered structures (e.g., Nabighian and Macnae, 1991; Wolfgram and Karlik, 1995; Green, 1998). On the other hand, a model that is more useful for interpretation of TEM soundings and, especially, airborne electromagnetic data is a conductive layer of finite thickness (i.e., a slab rather than a thin sheet). Immediately after the step change of the external source, the induced current is concentrated at the surface of the layer. This current decays with time and penetrates deeper into the layer. Eventually, the electric field is almost uniform across the layer. At this stage, the layer acts like a thin sheet with conductance

$$S = h\sigma_s, \tag{2}$$

where h and σ_s are the layer thickness and conductivity, respectively.

Maxwell's solution was derived assuming that the medium on both sides of the conductive thin sheet is an insulator. This restricts its application to interpretation of airborne data. Although the basement that underlies the conductive layer is often significantly more resistive than the layer, the induced current will nevertheless penetrate into it at late time. Eventually, the total current flowing in the basement will become comparable with and then larger than the current flowing in the layer. Thus, when Maxwell's solution is applied to a more practical two-layered model, its validity range is limited at early as well as late times. One of the goals of this paper is to evaluate limits of the thin sheet solution.

A straightforward numerical evaluation of electromagnetic response of a general 1D model requires finding the response function in the wavenumber-frequency domain ($\mathbf{k}$, ω), then carrying out a Fourier-Bessel (Hankel) transform from the wavenumber domain to the configuration space, and another Fourier transform from the frequency to the time domain. This procedure can be simplified in only few cases. For instance, Goldman and Fitterman (1987) analyzed the analytic properties of the ($\mathbf{k}$, ω)-response function and showed that for a conductive layer resting on a perfect conductor or a nonconductive half-space, the frequency-time domain transform can be calculated by summing up a series of terms decaying exponentially in time. A variety of approximate and asymptotic solutions can be used to accelerate the simulation for rather general 1D models (e.g., Wait, 1982, 210–216). The enormous amount of information acquired in an airborne survey and the necessity of a fast and reliable interpretation of this data justify a continuing search for rapid alternative algorithms. The simplicity and beauty of Maxwell's solution is a good incentive for finding a closed-form solution applicable to a two-layered model with a conductive upper layer.

A step in this direction has been made by Singer and Green (1998), who extended Maxwell's solution to a layer of finite thickness surrounded by an insulator. The extended solution is applicable at earlier times compared to the thin sheet solution. However, it does not consider electromagnetic induction in the basement. In this paper, we derive an upgraded asymptotic expression that accounts for both effects.

TIME-DOMAIN RESPONSE OF A TWO-LAYER MODEL

In this section, we outline the major steps leading to an exact expression for the time-domain response of a two-layer model shown in Figure 1. The expression will be analyzed and compared with the asymptotic solution derived in the next section.

The model under consideration comprises a homogeneous conductive layer of thickness h and conductivity σ_s. The layer rests on an infinite homogeneous basement. The conductivity of the basement is σ_b. In the Cartesian coordinate system, with OX- and OY-axes directed along the surface of the layer and the OZ-axis pointing downwards, the layer occupies the depth range $0 < z < h$; the basement coincides with the half-space $z > h$. The medium above the slab is assumed to be nonconductive. It is also assumed that the external source is located in the half-space $z < z_0$ ($z_0 < 0$), and that displacement currents can be ignored.

The electromagnetic field in a 1D medium can be described in terms of two scalar potentials (e.g., Weaver, 1970, 1994). A particular choice of the potentials is often a matter of convenience. In our consideration, we follow Vasseur and Weidelt (1977) in using the potentials that define toroidal and poloidal modes of the electromagnetic field. The electric field inside the conductor and the magnetic field in the whole space can be expressed as

$$\mathbf{E} = -\mu_0 \nabla \times \left(\mathbf{e}_z \frac{\partial V}{\partial t}\right) - \frac{1}{\sigma} \nabla \times \nabla \times (\mathbf{e}_z W) \tag{3}$$

and

$$\mathbf{H} = \nabla \times \nabla \times (\mathbf{e}_z V) - \nabla \times (\mathbf{e}_z W), \tag{4}$$

where potential V of the toroidal mode and potential W of the poloidal mode satisfy equations

$$\frac{\partial^2 V}{\partial z^2} + \nabla_\tau^2 V - \sigma \mu_0 \frac{\partial V}{\partial t} = 0 \tag{5}$$

and

$$\sigma \frac{\partial}{\partial z}\left(\frac{1}{\sigma}\frac{\partial W}{\partial z}\right) + \nabla_\tau^2 W - \sigma \mu_0 \frac{\partial W}{\partial t} = 0. \tag{6}$$

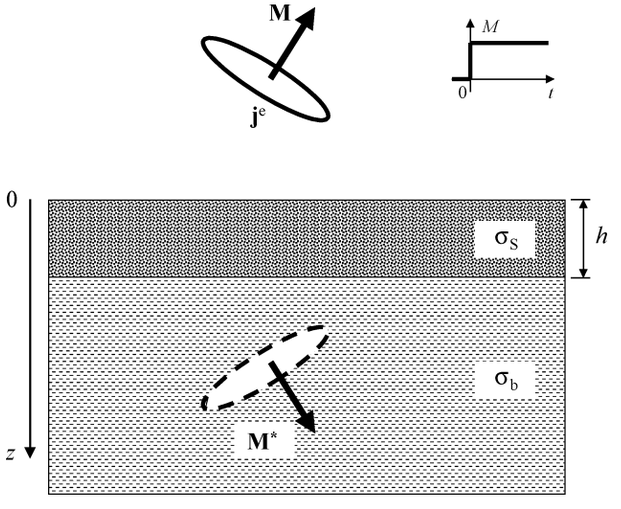

FIG. 1. A two-layer model is energized by an external airborne source. The conductive layer is of thickness h and conductivity σ_s; σ_b is the basement conductivity. The source magnetic moment $\mathbf{M}$ is turned on at $t = 0$; $\mathbf{M}^*$ is the magnetic moment of the imaginary dipole responsible for the secondary magnetic field in accordance with Maxwell's solution.

In these equations, $\nabla_\tau = \mathbf{e}_x(\partial/\partial x) + \mathbf{e}_y(\partial/\partial y)$ is the lateral part of the operator of spatial differentiation $\nabla = \nabla_\tau + \mathbf{e}_z(\partial/\partial z)$; $\mathbf{e}_x$, $\mathbf{e}_y$, and $\mathbf{e}_z$ are unit vectors of the Cartesian coordinate system; and $\sigma(z)$ is the conductivity distribution, which for the model under consideration represents a piece-wise constant function accepting values of 0, σ_s, and σ_b for $z<0$, $0<z<h$, and $z>h$, respectively.

The two field modes are independent outside the source. The electric field of the toroidal mode and the magnetic field of the poloidal field mode are confined to horizontal planes. It has been shown by Weaver (1973) that an external magnetic source does not excite the poloidal field mode in a stratified earth model. Therefore, $W=0$, and magnetic field is specified by the first term in the right side of equation (4).

In the free space below the source ($z_0<z<h$), potential V satisfies Laplace's equation, so that expression (4) is reduced to

$$\mathbf{H} = \nabla\frac{\partial V}{\partial z}. \tag{7}$$

In this paper it will be necessary to consider functions in space-time, space-frequency, wavenumber-time, and wavenumber-frequency domains. To simplify the notations, the same symbol will be used for a function and its Fourier transforms. When necessary, the original function and its transforms will be distinguished by their arguments. For instance, the original function $f(\mathbf{r}, z, t)$ and its Fourier transforms $f(\mathbf{r}, z, \omega)$ and $f(\mathbf{k}, z, t)$ are related as

$$\begin{aligned} f(\mathbf{r}, z, t) &= \int_{\Re} f(\mathbf{r}, z, \omega)e^{-\iota\omega t}\frac{dt}{2\pi}, \\ f(\mathbf{r}, z, t) &= \Im^{-1}[f(\mathbf{k}, z, t)] = \iint_{\Re^2} f(\mathbf{k}, z, t)e^{\iota\mathbf{k}\cdot\mathbf{r}}\frac{ds_{\mathbf{k}}}{(2\pi)^2}, \end{aligned} \tag{8}$$

where $\Im[\cdot]$ denotes the direct spatial Fourier transform, and $\mathbf{r} = x\mathbf{e}_x + y\mathbf{e}_y$ and $\mathbf{k} = k_x\mathbf{e}_x + k_y\mathbf{e}_y$ are the horizontal radius vector and wavenumber, respectively.

In the interval $z_0<z<0$, the solution of Laplace's equation for the potential

$$V(\mathbf{k}, z, \omega) = V^p(\mathbf{k}, 0, \omega)e^{-kz} + V^s(\mathbf{k}, 0, \omega)e^{+kz} \tag{9}$$

consists of the primary field (of the external source) decreasing downwards, and the secondary field decreasing upwards. At $z=0$, the secondary field can be expressed in terms of the primary field:

$$V^s(\mathbf{k}, 0, \omega) = -\gamma(k, \omega)V^p(\mathbf{k}, 0, \omega), \tag{10}$$

provided the reflection coefficient $\gamma(k, \omega)$ is known. Accordingly, the magnetic field is

$$\mathbf{H}(\mathbf{r}, z, \omega) = \mathbf{H}^p(\mathbf{r}, z, \omega) + \mathbf{H}^s(\mathbf{r}, z, \omega), \tag{11}$$

where its primary and secondary parts are

$$\mathbf{H}^p(\mathbf{r}, z, \omega) = -\nabla\Im^{-1}[kV^p(\mathbf{k}, 0, \omega)e^{-kz}] \tag{12}$$

and

$$\mathbf{H}^s(\mathbf{r}, z, \omega) = -\nabla\Im^{-1}[k\gamma(k, \omega)V^p(\mathbf{k}, 0, \omega)e^{+kz}], \tag{13}$$

respectively.

The reflection coefficient

$$\gamma(k, \omega) = \frac{\lambda^{-1}(k, \omega) - k}{\lambda^{-1}(k, \omega) + k} \tag{14}$$

can be expressed in terms of the response function

$$\lambda(k, \omega) = -\left[\frac{\partial}{\partial z}\ln V(\mathbf{k}, z, \omega)\right]^{-1}_{z=0+}, \tag{15}$$

which, in turn, is directly related to the toroidal mode impedance

$$Z^T(k, \omega) = -\iota\omega\mu_0\lambda(k, \omega). \tag{16}$$

For the two-layer model under consideration, the response function is

$$\lambda^{-1}(k, \omega) = \kappa_s(k, \omega)\frac{\kappa_b(k, \omega) + \kappa_s(k, \omega)\tanh[\kappa_s(k, \omega)h]}{\kappa_s(k, \omega) + \kappa_b(k, \omega)\tanh[\kappa_s(k, \omega)h]} \tag{17}$$

(Wait 1953), where $\kappa_s(k, \omega) = (k^2 - \iota\omega\mu_0\sigma_s)^{1/2}$ and $\kappa_b(k, \omega) = (k^2 - \iota\omega\mu_0\sigma_b)^{1/2}$.

After substitution of equation (17) in equation (14) and a straightforward transformation, the expression for the reflection coefficient can be reduced to

$$\begin{aligned} \gamma(k, \omega) = &-\frac{\iota\omega\mu_0}{\beta(k, \omega)} \\ &\times \frac{\sigma_b + [S\beta(k, \omega) - kh\sigma_b]\psi(k, \omega)}{\beta(k, \omega) + [kh\beta(k, \omega) - \iota\omega\mu_0 S]\psi(k, \omega)}, \end{aligned} \tag{18}$$

where S is the layer conductance as specified by equation (2) and

$$\begin{aligned} \beta(k, \omega) &= \kappa_b(k, \omega) + k, \\ \psi(k, \omega) &= \frac{\tanh[\kappa_s(k, \omega)h]}{\kappa_s(k, \omega)h}. \end{aligned} \tag{19}$$

It should be noted that equation (18) defines an exact reflection coefficient represented in a form convenient for further analysis. In particular, the reflection coefficient of the thin sheet model surrounded by a free space can be derived from equation (18) by setting $h=0$, $\sigma_b=0$, while retaining a finite value of S.

To consider a transient solution, it is assumed that the external source is turned on at $t=0$ and remains steady afterwards, i.e.,

$$\mathbf{H}^p(\mathbf{r}, z, t) = \mathbf{H}^p(\mathbf{r}, z, 0+)\Theta(t), \tag{20}$$

where $\Theta(t)$ is the Heaviside function. The corresponding expression for the primary field potential in the frequency domain is

$$V^p(\mathbf{k}, z, \omega) = \frac{\iota}{\omega}V^p(\mathbf{k}, z, 0+). \tag{21}$$

After an application of the inverse Fourier transform to equation (13), the expression for the secondary magnetic field is reduced to

$$\mathbf{H}^s(\mathbf{r}, z, t) = -\nabla\Im^{-1}[k\chi(k, t)V^p(\mathbf{k}, 0, 0+)e^{kz}], \tag{22}$$

where

$$\chi(k,t) = -\int_{-\infty}^{+\infty} \gamma(k,\omega) e^{-\iota\omega t} \frac{d\omega}{2\pi\iota\omega} \tag{23}$$

is the time-domain step-on response function.

Equation (23) can be simplified considering that from the causality principle, the reflection coefficient $\gamma(k,\omega)$ is a regular function of ω in the upper half of the complex ω-plane. Therefore, for $t>0$,

$$\int_{-\infty}^{+\infty} \gamma(k,\omega) e^{+\iota\omega t} \frac{d\omega}{2\pi\iota\omega} = 0. \tag{24}$$

Combining equations (23) and (24) and accounting for the fact that $\chi(k,t)$ is a real function and, therefore, $\mathrm{Re}\gamma(k,-\omega) = \mathrm{Re}\gamma(k,\omega)$, $\mathrm{Im}\gamma(k,-\omega) = -\mathrm{Im}\gamma(k,\omega)$, the step-on response function can be reduced to

$$\begin{aligned}\chi(k,t) &= \Theta(t)\frac{2}{\pi}\int_0^\infty \frac{\mathrm{Re}\gamma(k,\omega)}{\omega}\sin(\omega t)d\omega \\ &= \Theta(t)\sqrt{\frac{2t}{\pi}}\int_0^\infty \frac{\mathrm{Re}\gamma(k,\omega)}{\sqrt{\omega}} J_{1/2}(\omega t)d\omega,\end{aligned} \tag{25}$$

where J_ν is the νth order Bessel function of the first kind. The last integration can be efficiently carried out using the fast Hankel transform technique (e.g., Johansen and Sørensen 1979).

From equations (22) and (25),

$$\begin{aligned}\mathbf{H}^s(\mathbf{r},z,t) &= -\Theta(t)\sqrt{\frac{2t}{\pi}} \\ &\times\nabla\Im^{-1}\left[kV^p(k,0,0+)e^{kz}\int_0^\infty \frac{\mathrm{Re}\gamma(k,\omega)}{\sqrt{\omega}} J_{1/2}(\omega t)d\omega\right]\end{aligned} \tag{26}$$

represents the magnetic field of currents induced in the earth by the primary magnetic field

$$\mathbf{H}^p(\mathbf{r},z,t) = -\Theta(t)\nabla\Im^{-1}[kV^p(\mathbf{k},0,0+)e^{-kz}]. \tag{27}$$

If the external source is a magnetic dipole located at $x=y=0$, $z=z_0<0$, then the primary magnetic field is

$$\mathbf{H}^p(\mathbf{r},z,t) = \nabla\left(\frac{\mathbf{M}}{4\pi}\cdot\nabla\right)\frac{\Theta(t)}{\sqrt{r^2+(z-z_0)^2}}, \tag{28}$$

where $\mathbf{M}=\mathbf{M}_\tau + M_z\mathbf{e}_z$ is the is the magnetic moment of the dipole, and $\mathbf{M}_\tau$ and M_z are the horizontal and vertical components of the source magnetic moment. From equation (7), the vertical derivative of the primary toroidal potential

$$\frac{\partial V^p}{\partial z}(r,z,t) = \left(\frac{\mathbf{M}}{4\pi}\cdot\nabla\right)\frac{\Theta(t)}{\sqrt{r^2+(z-z_0)^2}}. \tag{29}$$

Using the well-known integral expressions (Erdélyi, 1953)

$$\begin{aligned}J_0(kr) &= \int_0^{2\pi} e^{\iota kr\cos\varphi}\frac{d\varphi}{2\pi}, \\ \frac{1}{\sqrt{r^2+z^2}} &= \int_0^\infty e^{-k|z|}J_0(kr)dk,\end{aligned} \tag{30}$$

it is easy to find from equation (29) that at the earth surface

$$kV^p(k,0,0+) = -\frac{1}{2}\left[\iota\frac{\mathbf{k}}{k}\cdot\mathbf{M} - M_z\right]e^{kz_0}. \tag{31}$$

Substitution of equation (31) reduces equation (26) for the secondary field to

$$\begin{aligned}\mathbf{H}^s(\mathbf{r},z,t) &= \nabla\left(\frac{\mathbf{M}^*}{2}\cdot\nabla\right)H_0\left[\chi(k,t)e^{k(z+z_0)}\right] = \Theta(t)\sqrt{\frac{2t}{\pi}} \\ &\times\nabla\left(\frac{\mathbf{M}^*}{2}\cdot\nabla\right)H_0\left[e^{k(z+z_0)}\int_0^\infty \frac{\mathrm{Re}\gamma_k(\omega)}{\sqrt{\omega}}J_{1/2}(\omega t)d\omega\right],\end{aligned} \tag{32}$$

where $\mathbf{M}^*=\mathbf{M}_\tau - M_z\mathbf{e}_z$ is the mirror image of the source magnetic dipole with respect to a horizontal plane and

$$H_0[f(k)] = \Im^{-1}\left[\frac{f(k)}{k}\right] = \int_0^\infty f(k)J_0(kr)\frac{dk}{2\pi} \tag{33}$$

denotes a zero-order Fourier-Bessel transform of an arbitrary function $f(k)$.

ASYMPTOTIC SOLUTION

Equation (32) presents an exact time-domain response of the two-layered model. We simplify this equation assuming that inside the essential parts of the wavenumber and frequency spectra

$$kh \ll 1 \tag{34}$$

and

$$|\kappa_s(0,\omega)h| = h\sqrt{\omega\mu_0\sigma_s} = \sqrt{\frac{h}{|\lambda_s(\omega)|}} \ll 1, \tag{35}$$

where $\lambda_s^{-1}(\omega) = -\iota\omega\mu_0 S$. The first of these conditions restricts the rate of spatial variations of the field in horizontal directions. The second condition restricts the rate of time variations, implying that the skin depth in the material of the layer is large compared to the layer thickness.

To estimate the time-domain solution at time t, attention should be directed at the behavior of the frequency-domain response at $\omega\sim 1/t$. The range of essential wavenumbers is controlled by the distance between the receiver and the image source. It is known from Maxwell's solution that the image source recedes downwards with the speed v_s specified by equation (1). Therefore, we have

$$\begin{aligned}\frac{h}{|\lambda_s(\omega)|} &= \omega\mu_0 Sh \sim \frac{\mu_0 Sh}{t} = \frac{2h}{v_s t}, \\ kh &\sim \frac{h}{\sqrt{r^2+(|z+z_0|+v_s t)^2}} < \frac{h}{v_s t},\end{aligned} \tag{36}$$

and conditions (34) and (35) are not independent. Both conditions are satisfied if

$$t \gg \frac{h}{v_s}. \tag{37}$$

This specifies the lower limit of the time range for applicability of the asymptotic solution. The upper limit is imposed by the assumption that the conductance of the energized part of the

basement is smaller than the layer conductance. At time t, most of the currents induced in the basement are restricted to the depth interval $h < z < h + \Lambda_0(t)$, where the diffusion distance (Wait, 1958; Ward and Hohmann, 1991) is

$$\Lambda_0(t) = \sqrt{\frac{2t}{\mu_0 \sigma_b}}. \tag{38}$$

Condition $\Lambda_0(t)\sigma_b \ll S$ is satisfied if

$$t \ll \frac{\mu_0 S^2}{2\sigma_b} = \frac{S}{\sigma_b v_s} = \left(\frac{\sigma_s}{\sigma_b}\right)\frac{h}{v_s}. \tag{39}$$

The time range specified by equations (37) and (38) is not empty if $\sigma_s \gg \sigma_b$ (i.e., the layer is significantly more conductive than the basement). In this time range, after neglecting function terms of the order of $(h/v_s t)^2$ or smaller, function $\psi(k, \omega)$, defined by equation (19), can be simplified as

$$\psi(k, \omega) \cong 1 - \frac{1}{3}\frac{h}{\lambda_s(\omega)}. \tag{40}$$

This equation, together with the inequality $k \gg \sigma_b/S$ for $k \sim 1/v_s t$, allows expression (18) for the reflection coefficient to be reduced to

$$\gamma(k, \omega) \cong -\iota\omega\mu_0 S \times \frac{1 + \dfrac{\iota\omega\mu_0 Sh}{3} + \dfrac{\alpha}{\beta(k,\omega)}(1 - kh)}{\beta(k, \omega)(1 + kh) - \iota\omega\mu_0 S\left(1 + \dfrac{\iota\omega\mu_0 Sh}{3}\right)}, \tag{41}$$

where $\alpha = \sigma_0/S$.

It is easy to see that this function is regular in the upper half of the complex ω-plane as it could be expected from the causality principle. In the lower half of the complex ω-plane, function $\gamma(k, \omega)$ has a branch point at

$$\omega^*(k) = -\iota\frac{k^2}{\mu_0 \sigma_b}. \tag{42}$$

This branch point is located on the negative part of the imaginary ω-axis (Figure 2). Outside the cut, that starts at the branch point and continues along the negative part of the imaginary ω-axis to infinity, $\gamma(k, \omega)$ is a regular function, except that it possesses a simple pole. Its location can be found by equating the denominator of equation (41) to zero. A straightforward consideration ignoring terms of the order of $(h/\lambda_s)^2$, $(\alpha/k)^2$, and $(h/\lambda_s)(\alpha/k)$ shows that the pole

$$\omega_0(k) = -\frac{\iota}{\mu_0 S}\left[2k\left(1 + \frac{1}{3}kh\right) - \alpha\right] \tag{43}$$

is located on the negative part of the imaginary ω-axis above the branch point.

After a substitution of equation (41), the step-on response function (23) can be estimated using the residue theorem as

$$\chi(k, t) = \operatorname*{Res}_{\omega=\omega_0(k)}\left[\frac{\gamma(k, \omega)}{\omega}e^{-\iota\omega t}\right] + \Phi(k, t), \tag{44}$$

where function $\Phi(k, t)$ represents the contribution of the integral along both sides of the cut in the complex ω-plane (Figure 2). The integration variable should be set to $\omega^*(k) + \eta e^{+\iota\frac{\pi}{2}}$ and $\omega^*(k) + \eta e^{-\iota\frac{\pi}{2}}$ on the left and right sides of the cut, respectively. After neglecting the terms related to the thickness of the layer,

$$\Phi(k, t) \cong \frac{4\alpha^2 k}{\pi}\int_0^\infty \frac{\eta^2 e^{-(k^2+\eta^2)\frac{t}{\mu_0\sigma b}}d\eta}{(k^2 + \eta^2)^2[(k - \alpha)^2 + \eta^2]} \le \frac{4}{\pi}\left(\frac{\alpha}{k}\right)^2\int_0^\infty \frac{k\eta^2 d\eta}{(k^2 + \eta^2)^2} = \left(\frac{\alpha}{k}\right)^2. \tag{45}$$

Therefore, for $k \gg \alpha$, the second term in the right side of equation (44) can be ignored. The contribution of the first term can be estimated as

$$\chi(k, t) \cong -\iota\mu_0 S \times \left[\frac{e^{-\iota\omega t}\left[1 + \dfrac{\iota\omega\mu_0 Sh}{3} + \dfrac{\alpha}{\beta(k,\omega)}(1 - kh)\right]}{\dfrac{\partial}{\partial\omega}\left[\beta(k, \omega)(1 + kh) - \iota\omega\mu_0 S\left(1 + \dfrac{\iota\omega\mu_0 Sh}{3}\right)\right]}\right]_{\omega=\omega_0(k)}. \tag{46}$$

A straightforward evaluation reduces this expression to

$$\chi(k, t) \cong \Theta_b(t)\left(1 - k^2\frac{hv_s t}{3}\right)e^{-k\left(v_s t + \frac{2}{3}h\right)}, \tag{47}$$

where function

$$\Theta_b(t) = \Theta(t)\left(1 + \frac{\sigma_b}{\mu_0 S^2}t\right) \tag{48}$$

equals zero for $t < 0$, and increases linearly for $t > 0$.

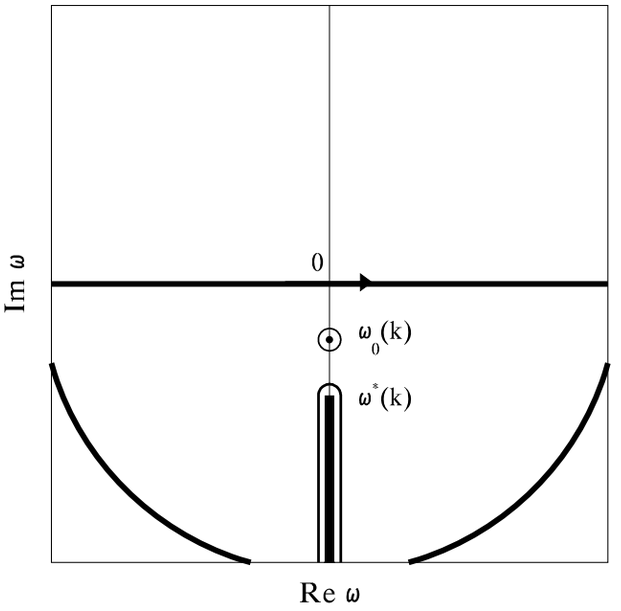

FIG. 2. Location of the singularities of the reflection coefficient $\gamma(k, \omega)$ in the complex ω-plane and the integration path.

A substitution of response function (47) into equation (32) results in the equation for the secondary magnetic field

$$\mathbf{H}^s(\mathbf{r},z,t) \cong \Theta_b(t)\left(1-\frac{hv_st}{3}\frac{\partial^2}{\partial z^2}\right) \times \nabla\left(\frac{\mathbf{M}^*}{2}\cdot\nabla\right)H_0\left[e^{k\left(z+z_0-\frac{2}{3}h-v_st\right)}\right]. \quad (49)$$

Using equation (30), this expression can be further reduced to

$$\mathbf{H}^s(r,z,t) \cong \Theta_b(t)\left(1-\frac{hv_st}{3}\frac{\partial^2}{\partial z^2}\right) \times \nabla\left(\frac{\mathbf{M}^*}{4\pi}\cdot\nabla\right)\frac{1}{\sqrt{r^2+\left(z+z_0-\frac{2}{3}h-v_st\right)^2}}. \quad (50)$$

Since any analytic function $f(z)$ can be approximated by a series, so that

$$\frac{1}{2}[f(z+\iota\eta)+f(z-\iota\eta)] = \left(1-\frac{\eta^2}{2}\frac{d^2}{dz^2}\right)f(z) + \frac{\eta^4}{4!}\frac{d^4f}{dz^4}+\cdots, \quad (51)$$

we can set $\eta=\sqrt{\frac{2}{3}hv_st}=2\sqrt{\frac{t}{3\mu_0\sigma_s}}$ and rewrite equation (50) in a form

$$\mathbf{H}^s(r,z,t) \cong \nabla\left(\frac{\mathbf{M}^*}{4\pi}\cdot\nabla\right) \times \mathrm{Re}\frac{\Theta_b(t)}{\sqrt{r^2+\left(z+z_0-\frac{2}{3}h-v_st+2\iota\sqrt{\frac{t}{3\mu_0\sigma_s}}\right)^2}}. \quad (52)$$

Equations (50) and (52) are valid in the time range $t_{\min} < t < t_{\max}$, where

$$t_{\min}=\frac{h}{v_s}, \qquad t_{\max}=\left(\frac{\sigma_s}{\sigma_b}\right)\frac{h}{v_s}. \quad (53)$$

For $h=0$ and $\sigma_b=0$, the asymptotic solution shows that the field of the induced current coincides with the field of an image dipole receding from its initial position at $x=y=0, z=-z_0>0$ downwards. Therefore, equation (52) complies with Maxwell's thin sheet solution. For $h>0$ and $\sigma_b=0$, it also answers the question that arises when the thin sheet solution is applied to a conductive layer of finite thickness, and it is then unclear what depth the equivalent thin sheet should be placed at. From equation (52), the thin sheet should be positioned at $z=h/3$, because the plane of symmetry is located at this depth immediately after the source is turned on.

To consider the effect of additional terms in equation (52), it is necessary to compare this equation with an exact secondary field. The numerically exact solution (32) requires evaluation of two successive Fourier-Bessel transforms, which can be carried out using one of the well-known fast Hankel transform algorithms (e.g., Johansen and Sørensen, 1979). We first consider three models with a nonconductive basement. The layer thickness in these models equals 10, 25, and 50 m, respectively. The primary field is generated by a vertical magnetic dipole at an altitude of 120 m. The vertical magnetic field is measured by a receiver at a height of 60 m. The horizontal separation between the source and the receiver is 100 m. Such a configuration is widely used in airborne electromagnetics (Palacky and West, 1991). Results of the numerical simulation are shown in three panels of Figure 3. In each panel, the dotted curve represents the relative error that occurs if the exact response $H_z^{s,L}$, specified by equation (32), is replaced by the response $H_z^{s,S}$ of the equivalent thin sheet (Maxwell's solution). The error is calculated as $(H_z^{s,S}/H_z^{s,L})-1$. The solid curves show the corresponding error $(H_z^{s,Sh}/H_z^{s,L})-1$ of the response $H_z^{s,Sh}$, calculated using equation (52) that accounts for the layer thickness.

As it can be seen from Figure 3, accounting for the layer thickness improves the solution at all times. Inside the time range (53), the relative error of the generalized solution does not exceed 0.12, 0.69, and 2.38% for layers with thickness of 10, 25, and 50 m, respectively. The maximum error is roughly proportional to h^2, which agrees with the fact that exact expression (18) for the reflection coefficient and its approximation (41) differ by the terms of order of $(h/v_st)^2$. It should be noted that the time scale used in Figure 3 is directly applicable to models with the conductance of layer equal to 1 S. The

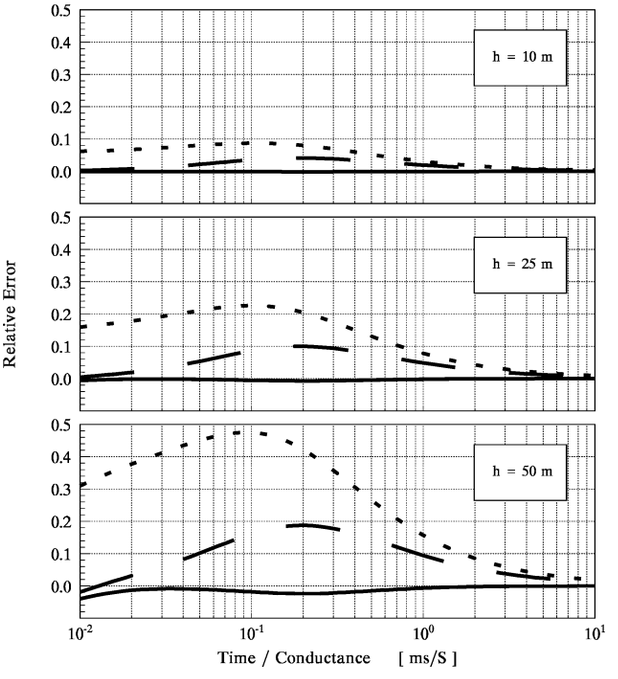

FIG. 3. Relative errors of the transient thin-sheet solution (dotted line), the shifted thin-sheet solution (dashed line), and the asymptotic solution accounting for the finite thickness of the conductive layer (solid line). The basement is nonconductive ($\sigma_b=0$). The solutions are compared with the numerically exact solution. The field is generated by a vertical magnetic dipole at the altitude of 120 m above the earth surface. The source is turned on at $t=0$ and remains constant afterwards. The receiver measures the vertical component of the secondary magnetic field at a height of 60 m and a horizontal separation of 100 m. The panels are for layer thickness $h=10$, 25, and 50 m, respectively.

curves should be shifted to the right if $S > 1$ S or to the left if $S < 1$ S by the factor of S or $1/S$, respectively.

Results for models with a basement of a finite conductivity are shown in Figure 4. The acquisition system and conductive layers are the same as in Figure 3. In all three models, the basement is assumed to be 100 times more resistive than the layer ($\sigma_s = 100\,\sigma_b$), which is typical for regolith-covered terrains (Worrall et al., 1999; Emerson et al., 2000). Each of the panels in Figure 4 displays three curves. The curves show the relative error of the thin sheet solution (dotted), the solution accounting for the layer thickness but ignoring induction in the basement (dashed), and the solution accounting for the layer thickness as well as conductivity of the basement (solid). It is clear from Figure 4 that ignoring currents induced in the resistive basement may lead to a significant error that increases with time as $(\sigma_b/\mu_0 S^2)t$. From Figure 4, the asymptotic solution (52), which accounts for the layer thickness as well as the conductivity of the basement, is far more accurate than the other approximations.

All the curves in Figures 3 and 4 are plotted for the t/S ratio in the range from 10 μs/S to 10 ms/S. The dynamic time range in which the asymptotic solution can be applied is controlled by the conductivity contrast σ_s/σ_b, as might be expected from equation (53). At the same time, the position of the range of applicability on the time scale is shifted to the shorter delays for a smaller layer thickness and to the longer delays for a larger layer thickness.

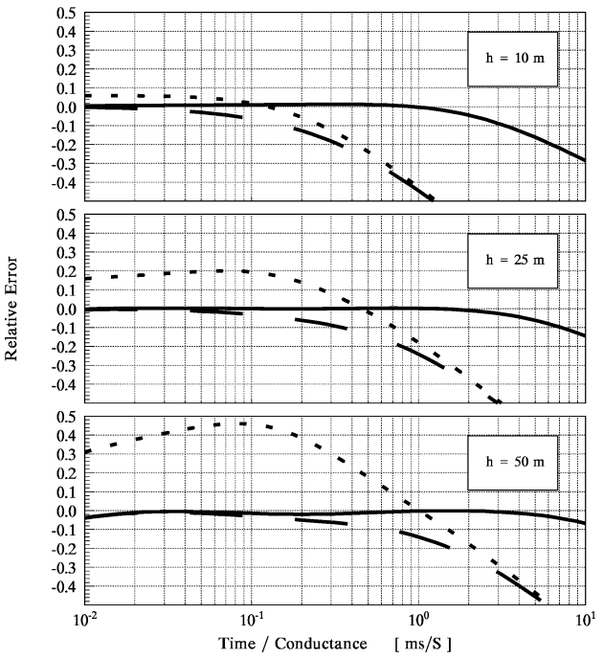

FIG. 4. Relative errors of the transient thin-sheet solution (dotted line), the asymptotic solution accounting for the finite thickness of the conductive layer and ignoring the basement conductivity (dashed line), and the asymptotic solution accounting for the finite thickness of the conductive layer and the conductivity of the basement (solid line). Parameters of the acquisition system are the same as in Figure 3. The layer is 100 times more conductive than the basement ($\sigma_s = 100\,\sigma_b$).

DISCUSSION AND CONCLUSIONS

Despite all the advantages of the thin sheet solution, some aspects of its practical application require clarification. Maxwell's solution is exact as long as the conductive layer is infinitely thin and surrounded by a free space. Even for a perfectly nonconducting basement, the same solution should be regarded as an asymptotic solution when it is applied to a more realistic model with a conductive layer of finite thickness. As for any asymptotic solution, it is important to know parameters that control the applicability range of this solution. Provided that the applicability range is established and the solution is applied within this range, it is also unclear where the equivalent thin sheet should be positioned.

Thus, a need for a better understanding of the opportunities and restrictions of the thin sheet solution represents a good impetus for looking beyond this solution. Another practical reason for an attempt to generalize Maxwell's solution is the fact that an interpretation based on the thin sheet solution can determine only conductance of the layer; neither the layer thickness nor its conductivity can be independently resolved. This limitation is inherently associated with the thin sheet model because the secondary magnetic field induced in such a model depends only on the source altitude and the layer conductance.

Our consideration of a model comprising a conductive layer and a resistive basement reveals two small parameters. The first parameter $\alpha_1 = h/v_s t$, where v_s is the recession speed of the image source. If α_1 is small, the distribution of the currents induced in the layer is almost uniform across this layer. Another small parameter $\alpha_2 = \sigma_b v_s t/S$, where S and σ_b are the layer conductance and conductivity of the basement. If α_2 is small, the magnetic field of currents in the basement is small compared to that of currents in the layer.

The thin sheet solution ignores the terms of the order of α_1 and α_2. Therefore, for the solution to be valid, inequalities $\alpha_1 \lesssim \varepsilon$ and $\alpha_2 \lesssim \varepsilon$ (where the symbol "$\lesssim$" means "less than or of the order of," and ε is the required accuracy of the computation) should be satisfied. From these conditions, one can expect that Maxwell's solution is applicable inside the time range $t_{\min}\varepsilon^{-1} \lesssim t \lesssim t_{\max}\varepsilon$, where $t_{\min}$ and $t_{\max}$ are defined by equation (53). It is clear that for the thin sheet solution to be applicable, the layer should be significantly more conductive than the basement (i.e., $\sigma_s \gtrsim \sigma_b \varepsilon^{-2}$). For instance, if the layer is only 25-m thick and 100 times more conductive than the basement, the thin sheet solution can hardly be used even if such a moderate accuracy as $\varepsilon = 0.1$ is required (for the airborne configuration used in the previous section).

The generalized solution accounts for finite thickness of the layer as well as conductivity of the resistive basement. This is achieved by retaining terms of the order of α_1 and α_2. The second-order terms are neglected. Thus, it is necessary to satisfy inequality $\max\{\alpha_1^2, \alpha_1\alpha_2, \alpha_2^2\} \lesssim \varepsilon$ in order to preserve the required accuracy of the response. The solution is valid in the time range $t_{\min}\varepsilon^{-1/2} \lesssim t \lesssim t_{\max}\varepsilon^{+1/2}$. This time range is not empty if $\sigma_s \gtrsim \sigma_b \varepsilon^{-1}$. The time range of the new solution is wider and the restriction on the conductivity contrast is less severe compared to the classic solution. The examples in the previous section show that even at accuracy $\varepsilon = 0.025$, the solution remains valid for $t_{\min} < t < t_{\max}$, which is even wider than expected.

The generalized solution is a closed-form asymptotic solution, which is also expressed in terms of the image source

receding downwards from the conductive layer. The time necessary for a numerical evaluation of the generalized response is comparable with the time required for the thin sheet solution. Depending on the length of the fast Hankel transform filters used for calculation of the exact response, the generalized solution is many hundred to several thousand times faster than the exact solution.

A byproduct of the new solution is the specification of the position of the equivalent thin sheet. Correct positioning of the thin sheet has a rather strong effect on the accuracy of the solution. Dashed curves in Figure 3 show the relative error calculated for Maxwell's solution with the thin sheet placed at the correct position. In the considered time range, this thin sheet approximates the layer better than a thin sheet placed at the top of the conductive layer. Unfortunately, in a typical airborne survey, the altitude of the acquisition system with respect to the top of the conductive layer may be unknown and has to be considered as one of the inversion parameters. If this is the case, the layer thickness cannot be distinguished from other geometrical parameters. In this respect, the new solution offers new opportunities. The secondary magnetic field in this solution explicitly depends on the layer thickness and conductivity. These parameters as well as the conductivity of the basement can potentially be resolved.

The earliest time $t_{\min}$ when the new solution can be used at is specified by the time necessary for Maxwell's image dipole to cross the layer. The latest time $t_{\max}$ is directly proportional to the conductivity contrast between the layer and the basement. Considering that even a closed-form TEM solution for a magnetic dipole elevated above a homogeneous half-space is unknown, it is hard to expect that our solution can be easily expanded beyond $t_{\max}$. On the other hand, the solution may be extended to earlier times. Indeed, immediately after the source is turned on, the induced currents flow at the earth surface. As long as these currents remain at a shallow depth, the secondary magnetic field is not sensitive to the details of the conductivity distribution in the earth. Not surprisingly, Maxwell's solution for the thin sheet placed at the earth surface is accurate at the early times (dotted curves in Figure 5). At early times, the new solution behaves similarly to the shifted thin-sheet solution (i.e., with the thin sheet positioned at $z = h/3$), which appears less accurate (dashed curves in Figure 5). It is easy to see that the deterioration of the accuracy of the new solution at the early time occurs owing to the same shift in the position of the equivalent thin sheet to which the improved accuracy in the time range $t_{\min} < t < t_{\max}$ is attributed. It is, therefore, possible to improve the early time behavior of the new solution by replacing the $(2/3)h$ term with an expression that accepts the necessary value for $t_{\min} < t < t_{\max}$ and disappears as $t \to 0$. For instance, function

$$d(t) = \frac{\delta(t)}{\tanh \dfrac{h}{\delta(t)}}, \tag{54}$$

where

$$\delta(t) = \sqrt{\frac{t}{\mu_0 \sigma}} = \sqrt{\frac{1}{2} h v_s t}, \tag{55}$$

satisfies this requirement. Indeed, for $t \gg t_{\min}$, $\delta(t) \gg h$ and $d(t) \cong (1/2)v_s t + (1/3)h$. On the other hand, for $t \ll t_{\min}$, $\delta(t) \ll h$ and $d(t) \cong \delta(t)$, which fits with the simple behavior of the image prescribed by Macnae and Lamontagne (1987). Using this definition, equation (52) for the secondary magnetic field can be modified to

$$H^s(r, z, t) \cong \nabla\left(\frac{\mathbf{M}^*}{4\pi} \cdot \nabla\right) \times \mathrm{Re}\frac{\Theta_b(t)}{\sqrt{r^2 + \left(z + z_0 - 2d(t) + \dfrac{2\iota}{\sqrt{3}}\delta(t)\right)^2}}. \tag{56}$$

In the extended time range $0 < t < t_{\max}$, the relative error of solution (56) does not exceed 1.05, 2.22, and 4.04% for the layers with the thickness of 10, 25, and 50 m, respectively. This solution is more accurate than the thin sheet solution or the solution specified by equation (52). Corresponding results, calculated for the acquisition system and the set of three models used in the previous section, are shown in Figure 5.

For practical applications it is convenient to carry out the differentiation implied in equations (28) and (56). A straightforward differentiation reduces expressions for the primary and secondary magnetic fields to

$$\mathbf{H}^p(\mathbf{r}, z, t) = \Theta(t)\hat{\mathbf{G}}(\mathbf{r}, z - z_0)\mathbf{M} \tag{57}$$

and

$$\mathbf{H}^s(\mathbf{r}, z, t) \cong \Theta_b(t)\,\mathrm{Re}\,\hat{\mathbf{G}}\left(\mathbf{r}, z + z_0 - 2d(t) + \frac{2\iota}{\sqrt{3}}\delta(t)\right)\mathbf{M}^*, \tag{58}$$

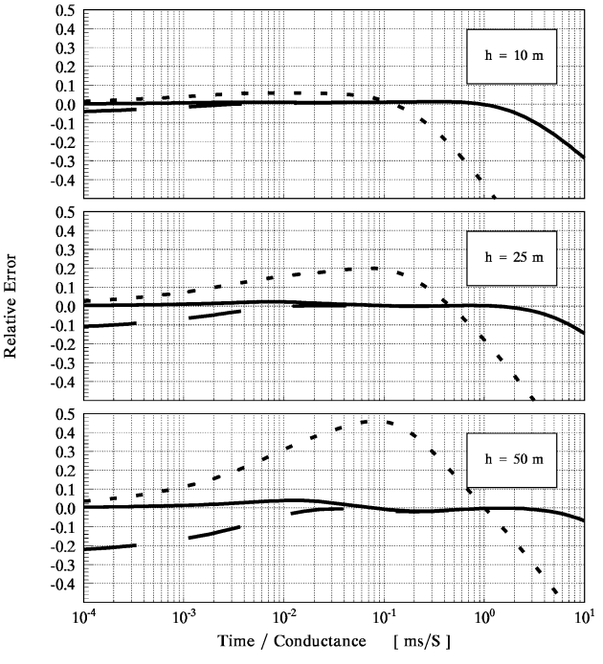

FIG. 5. Relative errors of the transient thin-sheet solution (dotted line), the asymptotic solution accounting for the finite thickness of the conductive layer and the basement conductivity (dashed line), and the asymptotic solution with the corrected behavior at early times (solid line). The models and the acquisition system are the same as in Figure 4.

where matrix

$$\hat{\mathbf{G}}(\mathbf{r}, z) = \frac{1}{4\pi R^3}\begin{pmatrix} 3\xi^2 - 1 & +3\xi\eta & -3\xi\zeta \\ +3\xi\eta & 3\eta^2 - 1 & -3\eta\zeta \\ -3\xi\zeta & -3\eta\zeta & 3\zeta^2 - 1 \end{pmatrix}, \quad (59)$$

and $\xi = \frac{x}{R}$, $\eta = \frac{y}{R}$, $\zeta = \frac{z}{R}$, $R = \sqrt{x^2 + y^2 + z^2}$.

In conclusion, it is worth noticing that despite the fact that throughout our consideration the layer was assumed to be thin, the terms correcting Maxwell's solution for finite thickness of the layer cannot be derived from the generalized thin-sheet approximation (Dmitriev, 1969; Ranganayaki and Madden, 1980). As discussed by Singer and Fainberg (1999), the generalized thin-sheet approximation is the first-order approximation with respect to small parameters $h\sqrt{\omega\mu_0\sigma} \sim \sqrt{h/v_s t}$ and h/λ_τ, where λ_τ is the characteristic length of the field variations along the surface of the layer. These parameters are generally independent. In the problem discussed in this paper, both parameters are controlled by the elapsed time after the source has been switched on. As a result, a single small parameter becomes responsible for the accuracy of the approximation, and a higher order approximation should be considered. The terms of the order of $h/v_s t$ play the major role in our consideration. These terms are beyond the limits of the generalized thin-sheet approximation.

ACKNOWLEDGMENTS

The authors are grateful to D. Fitterman, J. T. Weaver, P. Weidelt, and anonymous reviewers for numerous suggestions and comments that greatly contributed to improvement of the manuscript. We also thank E. Zinger for help in preparing the manuscript.

REFERENCES

Dmitriev, V. I., 1969, Approximate boundary conditions at a thin inhomogeneous layer in electrical exploration problems: Physics of the Solid Earth, **12**, 757–758.

Emerson, D., Macnae, J., and Sattel, D., 2000, Physical properties of the regolith in Lawlers area, Western Australia: Expl. Geophys., **31**, 229–235.

Erdélyi, A., Ed., 1953, Higher transcendental functions: McGraw-Hill Book Co., Inc.

Goldman, M. M., and Fitterman, D. V., 1987, Direct time-domain calculation of the transient response for a rectangular loop over a two-layer medium: Geophysics, **52**, 997–1006.

Green, A., 1998, Amplitude correction of time domain AEM data for image display and geological mapping using the apparent dipole depth (ADD) method: Expl. Geophys., **29**, 87–91.

Johansen, H. K., and Sørensen, K., 1979, Fast Hankel transform: Geophys. Prosp., **27**, 876–901.

Macnae, J., and Lamontagne, Y., 1987, Imaging quasi-layered conductive structures by simple processing of transient electromagnetic data: Geophysics, **52**, 545–554.

Maxwell, J. C., 1954, A treatise on electricity and magnetism: Dover Publication, **2**.

Nabighian, M. N., and Macnae, J. C., 1991, Time domain electromagnetic prospecting methods, *in* Nabighian, M. N., Ed., Electromagnetic methods in applied geophysicists: Soc. Expl. Geophys., **2**, 427–479.

Palacky, G. J., and West, G. F., 1991, Airborne electromagnetic methods, *in* Nabighian, M. N., Ed., Electromagnetic methods in applied geophysics: Soc. Expl. Geophys., **2**, 811–879.

Ranganayaki, R. P., and Madden, T. R., 1980, Generalised thin sheet analysis in magnetotellurics: An extension of Price's analysis: Geophys. J. Roy. Astr. Soc., **60**, 445–457.

Singer, B. Sh., and Fainberg, E. B., 1999, Modelling electromagnetic fields in thin heterogeneous layers with application to field generation by volcanoes—I. Theory and example: Geophys. J. Internat., **138**, 125–145.

Singer, B. Sh., and Green, A., 1998. Generalisation of the transient field solution for a thin layer of finite thickness: Explor. Geophys., **29**, 195–197.

Vasseur, G., and Weidelt, P., 1977, Bimodal electromagnetic induction in non-uniform thin sheet with application to the northern Pyrenean induction anomaly: Geophys. J. Roy. Astr. Soc., **51**, 669–690.

Wait, J. R., 1953, Propagation of radio waves over a stratified ground: Geophysics, **18**, 416–422.

——— 1958, Propagation of electromagnetic pulses in homogeneous conductive earth: App. Sci. Res., **B3**, 279–292.

——— 1982, Geo-electromagnetism: Academic Press Inc.

Ward, S. H., and Hohmann, G. W., 1991, Electromagnetic theory for geophysical applications, *in* Nabighian, M. N., Ed., Electromagnetic methods in applied geophysics: Soc. Expl. Geophys., **1**, 131–311.

Weaver, J. T., 1970, The general theory of electromagnetic induction in conducting half-space: Geophys. J. Roy. Astr. Soc., **22**, 83–100.

——— 1973, Induction in a layered plane earth by uniform and non-uniform source fields: Phys. Earth Plan. Int., **7**, 266–281.

——— 1994, Mathematical methods for geo-electromagnetic induction: John Wiley & Sons, Inc.

Wolfgram, P., and Karlik, G., 1995, Conductivity-depth transform of GEOTEM data: Expl. Geophys., **26**, 179–185.

Worrall, L., Munday, T., and Green, A., 1999, Beyond bump finding—Airborne electromagnetics for mineral exploration in regolith dominated terrains: Expl. Geophys., **29**, 199–201.